



Crystal structure of *cis*-dihydrodiol naphthalene dehydrogenase (NahB) from *Pseudomonas* sp. MC1: Insights into the early binding process of the substrate



Ae Kyung Park^a, Hyun Kim^a, Il-Sup Kim^b, Soo Jung Roh^{a,c}, Seung Chul Shin^a, Jun Hyuck Lee^{a,d}, Hyun Park^{a,d}, Han-Woo Kim^{a,d,*}

^a Unit of Polar Genomics, Korea Polar Research Institute, Incheon 21990, South Korea

^b School of Life Sciences, BK21 Plus KNU Creative BioResearch Group, Kyungpook National University, Daegu 41566, South Korea

^c Evolutionary Genomics Laboratory, Department of Biological Sciences, Inha University, 100 Inha-ro, Nam-gu, Incheon, 22212, South Korea

^d Department of Polar Sciences, University of Science and Technology, Incheon 21990, South Korea

ARTICLE INFO

Article history:

Received 12 July 2017

Accepted 14 July 2017

Available online 17 July 2017

Keywords:

Naphthalene

Degradation

Cis-dihydrodiol naphthalene dehydrogenase

Antarctica

Pseudomonas sp.

2,3-Dihydroxybiphenyl

ABSTRACT

The bacterial strain *Pseudomonas* sp. MC1 harbors an 81-kb metabolic plasmid, which encodes enzymes involved in the conversion of naphthalene to salicylate. Of these, the enzyme NahB (*cis*-dihydrodiol naphthalene dehydrogenase), which catalyzes the second reaction of this pathway, binds to various substrates such as *cis*-1,2-dihydro-1,2-dihydroxy-naphthalene (1,2-DDN), *cis*-2,3-dihydro-2,3-dihydroxybiphenyl (2,3-DDB), and 3,4-dihydro-3,4-dihydroxy-2,2',5,5'-tetrachlorobiphenyl (3,4-DD-2,2',5-5-TCB). However, the mechanism underlying its broad substrate specificity is unclear owing to the lack of structural information. Here, we determined the first crystal structures of NahB in the absence and presence of NAD⁺ and 2,3-dihydroxybiphenyl (2,3-DB). Structure analysis suggests that the flexible substrate-binding loop allows NahB to accommodate diverse substrates. Furthermore, we defined the initial steps of substrate recognition and identified the early substrate-binding site in the substrate recognition process through the complex structure with ligands.

© 2017 Elsevier Inc. All rights reserved.

1. Introduction

Polycyclic aromatic hydrocarbons (PAHs), comprising two or more benzene rings, are one of the most widespread organic pollutants. PAHs are typically formed during the incomplete burning of organic materials such as wood, coal, and oil gasoline [1]. There are more than 100 different PAH compounds that persist for longer time in the environment, owing to their low solubility in water and absorption onto solid particles [2]. Their toxicity and mutagenic and carcinogenic properties are raising several environmental concerns [3]. Therefore, there is an increasing interest in understanding the processes of degradation or detoxification of these compounds by physicochemical and microbial methods. Biological processes are known to completely degrade the pollutants at low cost and deemed safe. As a result, biological processes are more

applicable for the treatment of contaminated PAHs than physicochemical treatment [4].

Naphthalene (C₁₀H₈; CAS number 91-20-3), one of the most widespread environmental pollutants, is the simplest PAH formed by two aromatic rings that share two carbon atoms [5]. Based on its abundance and toxicity, naphthalene is identified as a priority pollutant and stated to be a possible human carcinogen by the Environmental Protection Agency of the USA [6]. Due to its high solubility and simplest structure, naphthalene has been used as a model compound for studies on the degradation metabolism of PAHs by microorganisms [7]. Degradation of naphthalene has been extensively studied in gram-negative bacteria such as *Pseudomonas* [8] and *Ralstonia* species [9]. In *Pseudomonas putida* G7, the naphthalene degradation pathway genes are found to be organized in the plasmid pNAH7 [10]. The naphthalene-degrading bacterium *Pseudomonas* sp. MC1 strain was recently isolated at the King Sejong Station (62°13'S58°47'W) on King George Island, Antarctica [11]. The strain MC1 also harbors a plasmid pYIC1 carrying genes for naphthalene degradation. Plasmids of both G7 and MC1 strains exhibit two operons associated with naphthalene degradation,

* Corresponding author. Unit of Polar Genomics, Korea Polar Research Institute, Incheon 21990, South Korea.

E-mail address: hwkim@kopri.re.kr (H.-W. Kim).

with almost identical protein-coding sequence. The first operon includes the naphthalene degradation upper-pathway (*nah*) genes for the conversion of naphthalene to salicylate, while the second operon includes the genes responsible for the conversion of salicylate to pyruvate and acetyl coenzyme A via catechol production [12]. In *Ralstonia* sp. strain U2, the *nag* genes code for all enzymes in only one operon; these enzymes convert naphthalene to pyruvate and fumarate via salicylate (2-hydroxybenzoate) and gentisate (2,5-dihydroxybenzoate) [13,14]. Although these operons differ in their structures, the first step of naphthalene degradation is catalyzed by naphthalene dioxygenase complex (NahAaAbAcAd) to yield *cis*-1,2-dihydroxy-1,2-dihydronaphthalene (*cis*-naphthalene dihydrodiol, 1,2-DDN) [15]. The second step is the conversion of 1,2-DDN to 1,2-dihydroxynaphthalene (1,2-DN) by *cis*-1,2-dihydro-1,2-dihydroxynaphthalene dehydrogenase (*cis*-dihydrodiol naphthalene dehydrogenase, NahB, EC 1.3.1.29) in presence of nicotinamide adenine dinucleotide (NAD⁺) as an electron acceptor [16].

Several reports have suggested that NahB exhibits relaxed substrate specificity and displays the ability to oxidize different *cis*-dihydrodiols beyond their natural substrates [16–20]. However, the molecular mechanism underlying the broad substrate specificity of NahB is still elusive. In this direction, we determined the crystal structures of NahB from *Pseudomonas* sp. MC1. Moreover, we compared NahB structures in their apo form and as complexes with NAD⁺ and 2,3-dihydroxybiphenyl (2,3-DB). Our results will improve the understanding of NahB-mediated reaction mechanism, which may help in NahB enzyme engineering for the bioremediation of toxic compounds.

2. Materials and methods

2.1. Reverse transcription polymerase chain reaction (RT-PCR)

For RT-PCR, *Pseudomonas* sp. MC1 cells were grown at 15 °C in R2A medium in the presence or absence of naphthalene (30 mg/L) [21]. Total RNA was purified with an easy-spin (DNA free) Total RNA Extraction Kit (iNtRON, South Korea). Complementary DNAs (cDNAs) were synthesized using M-MLV reverse transcriptase kit (Enzynomics, South Korea). The 16S rRNA was used as a control.

2.2. Recombinant protein expression, purification, and crystallization

The *nahB* gene from *Pseudomonas* sp. MC1 was cloned into the pKM260 vector (Euroscarf, Germany) between *Nco*I and *Bam*HI restriction sites with an N-terminal hexahistidine tag. The recombinant plasmid was transformed into the *Escherichia coli* BL21 (DE3) for protein expression. The cells were grown in Luria-Bertani medium containing 50 mg/mL ampicillin until an OD₆₀₀ of 0.6 was reached. The culture was induced at 25 °C with 0.2 mM isopropyl β-D-1-thiogalactopyranoside (IPTG) for 12 h. Following protein expression, the cell pellet was resuspended in buffer A (20 mM Tris-Cl pH 8 and 200 mM sodium chloride [NaCl]) and lysed by sonication. The supernatant obtained after centrifugation was loaded onto a column charged with Ni²⁺-chelated resin. The column was washed with buffer B (20 mM Tris-HCl pH 8, 200 mM NaCl, and 30 mM imidazole) and the protein eluted with buffer C (20 mM Tris-HCl pH 8, 200 mM NaCl, and 300 mM imidazole). The eluted fraction was further purified using a HiLoad 16/60 Superdex 200 column (GE Healthcare, USA), which was pre-equilibrated with buffer A. The protein concentration was determined from its absorbance at 280 nm wavelength. The protein was subsequently concentrated to 20 mg/mL by ultracentrifugation using a 10-kDa molecular-weight cutoff spin concentrator (Millipore, USA). For apo crystals of NahB, initial crystallization screening was

performed by the sitting-drop vapor-diffusion method using crystallization screening kits. Commercial screening kits such as PEG/Ion, PEGRx, Index (Hampton Research, USA), and MCSG Crystallization Suite (Anatrace, USA) were utilized. Each crystallization drop was prepared by equilibrating the mixture of 0.5 μL reservoir solution and 0.5 μL protein solution against 70 μL reservoir solution. Crystals were obtained under conditions comprising 0.1 M Tris-Cl pH 8.0, 0.2 M calcium chloride (CaCl₂), and 20% polyethylene glycol (PEG) 6000. For co-crystallization, the protein was incubated with 5 mM NAD⁺ and 5 mM 1,2-DN or 2,3-DB for 30 min on ice. Initial crystallization screening was performed with 96-well plates, using commercial screening kits. A good quality of complex crystals with NAD⁺ and 2,3-DB were obtained using 0.1 M ammonium citrate tribasic pH 7.0 and 12% PEG 3350.

2.3. Structure solution and refinement

For cryoprotection, crystals were transferred to perfluoropolyether oil PFO-X175/08 (Hampton Research) and flash frozen in a liquid-nitrogen stream. Diffraction data of apo and ternary complex crystals with NAD⁺ and 2,3-DB were collected using an ADSC Quantum 315 CCD detector on beamline 5C at the Pohang Light Source (Pohang, South Korea). X-ray diffraction data were collected to a resolution of 2.1 and 2.3 Å from the apo and ternary complex crystals, respectively. Datasets were indexed, processed, and scaled using the *HKL-2000* software package [22]. The crystal structure of apo NahB was solved by the molecular replacement (MR) method using the *MOLREP* program in the *CCP4* package [23] with *cis*-2,3-dihydro-2,3-dihydroxybiphenyl dehydrogenase (BphB, PDB ID: 2Y93) as a search model [20]. Refinement was performed using *Refmac5* [24] and the model was rebuilt with the *COOT* program [25]. The resulting structure of apo NahB was subsequently used as search model for the complex structures in NAD⁺ and 2,3-DB. Stereochemical qualities for all of the final models were deemed excellent, as assessed by *MolProbity* [26]. Data collection and refinement statistics are summarized in Table 1. All structural figures were generated using the *PyMOL* program [27].

2.4. Protein data bank accession number

The coordinates of the structures together with the structure factors have been deposited in the Protein Data Bank (<http://www.rcsb.org/pdb>) with accession codes 5XTF and 5XTG.

3. Results and discussion

3.1. Inducible expression of *nahB* gene by naphthalene

Pseudomonas sp. MC1 was isolated from wastewater treatment facility of the King Sejong Station. The plasmid from the strain MC1 has naphthalene degradation operon similar to that of the plasmid pNAH7 from *P. putida* G7 [10], which has been known to degrade naphthalene [11]. To confirm that the naphthalene degradation operon is activated by the inducer, we monitored the expression level of *nahB* gene in the absence and presence of naphthalene as the substrate. MC1 cells were grown with or without naphthalene at 15 °C for about 2 days. As shown in Fig. 1A, mRNA synthesis of *nahB* was increased in presence of naphthalene, suggesting that naphthalene may induce the degradation pathway in MC1 cells.

3.2. Overall structure

The crystal structure of NahB was determined in the absence and presence of NAD⁺ and 2,3-DB at resolutions of 2.1 and 2.3 Å,

Table 1

Data collection and refinement statistics.

	NahB	NahB_NAD ⁺ _2,3-DB
<i>Data collection</i>		
Space group	P 2 21 21	P 42 21 2
Cell dimension (Å)	a = 63.162, b = 69.695, c = 117.692	a = b = 70.082, c = 119.181
Resolution range (Å)	50–2.1 (2.14–2.1)	50–2.3 (2.34–2.3)
Total reflections	179,562	305,059
Unique reflections	35,667 (2665)	13,462 (1309)
Redundancy	6.1 (3.0)	22.5 (15.3)
Completeness (%)	94.5 (73.9)	97.7 (60.4)
R _{merge} (%)	10.7 (30.4)	15.3 (33.0)
$\langle I/\sigma(I) \rangle$	14.0 (1.8)	58.9 (3.8)
<i>Refinement</i>		
R _{factor} /R _{free} (%)	20.3/23.8	17.4/22.5
RMS deviation of		
Bond length (Å)	0.009	0.012
Bond angle (°)	1.01	1.26
<i>In Ramachandran plot</i>		
Most favored (%)	96	96
Additionally allowed (%)	4.2	3.5

The values in parentheses refer to the highest resolution shell.

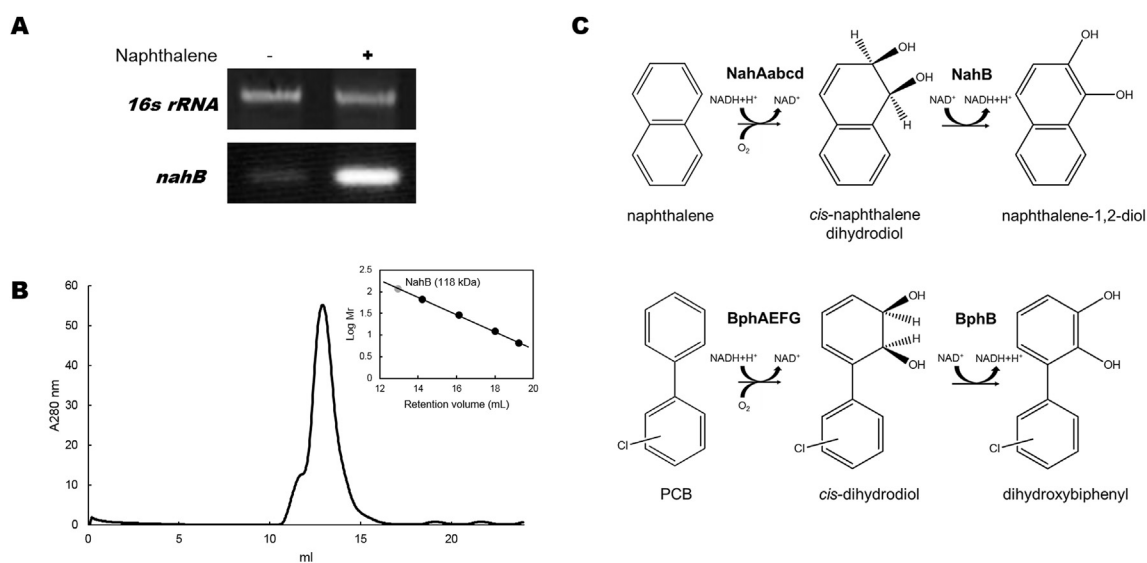
R_{factor} = $\sum |F_o| - |F_c| / \sum |F_o|$. A 5% reflection was used for R_{free} calculations.

Fig. 1. A. Analysis of the expression of *nahB* in presence of naphthalene. *Pseudomonas* sp. MC1 was grown in the absence or presence of naphthalene and total RNA isolated. B. Analytical size-exclusion chromatography of NahB (residues 1–259; calculated molecular weight of tetrameric NahB is 118 kDa, including tags for the polypeptide chain). The molecular mass of recombinant NahB was determined by the analysis of the elution of standard proteins from a Superdex 200 10/300 GL column (GE Healthcare, USA). The column was calibrated with molecular mass standards: albumin (66 kDa), carbonic anhydrase (29 kDa), cytochrome C (12.4 kDa), and aprotinin (6.5 kDa). C. Schematic representation of the aerobic degradation of naphthalene and polychlorinated biphenyl (PCB).

respectively. There were two and one NahB in the asymmetric unit of the apo and ligand-complex structures, respectively. Superposition of the apo and complex structure of NahB revealed no significant structural differences. NahB belongs to dihydrodiol dehydrogenases, which degrades monoaromatic compounds, biphenyl, and naphthalene and all of these enzymes were found to be tetrameric [16,28–30]. This is in line with our results obtained using analytical size-exclusion chromatography (Fig. 1B). Structural comparison between NahB and other proteins using the DALI server [31] indicated that BphB from *Pandoraea pnomenusa* and NahB display the same fold (Fig. 1C) [20]. Previous reports showed that NahB and BphB exhibited common features such as the absolute requirement for NAD⁺ and similar substrate spectrum [16,17]. Although these enzymes share 34% sequence identity, multiple sequence alignment indicated that the amino acids at their cofactor- and substrate-binding sites are well conserved (Fig. S1). The complete structure of BphB comprises three parts as

follows: the main body adopting Rossmann-fold (Met1-Gly186 and Leu217-Tyr251), the substrate-binding loop (Met187-Val216), and the C-terminal region (Asp252-Ile275) [20]. In particular, the substrate-binding loop of BphB was absent in the apo and complex structure of NahB, but visible in the ternary complex structure with NAD⁺ and products (2,3-DB and 4,4-dihydroxybiphenyl [4,4-DB]). As shown in Fig. 2A, NahB also adopts Rossmann-fold (Met1-Val186 and Leu215-Lys259) with seven-stranded parallel β -sheet (β 1– β 7) surrounded by three α -helices on either side. The structure of NahB indicated that the substrate-binding loop (Thr187-Gly214) is disordered in the absence of the ligand. The ternary structure of NahB in complex with NAD⁺ and 2,3-DB showed that the substrate-binding loop remains disordered even in the presence of the ligand. Comparison of the C-terminal region revealed that BphB displays an extended loop and small helices, but NahB has no C-terminal region.

Both NahB and BphB exist as dimers in an asymmetric unit and

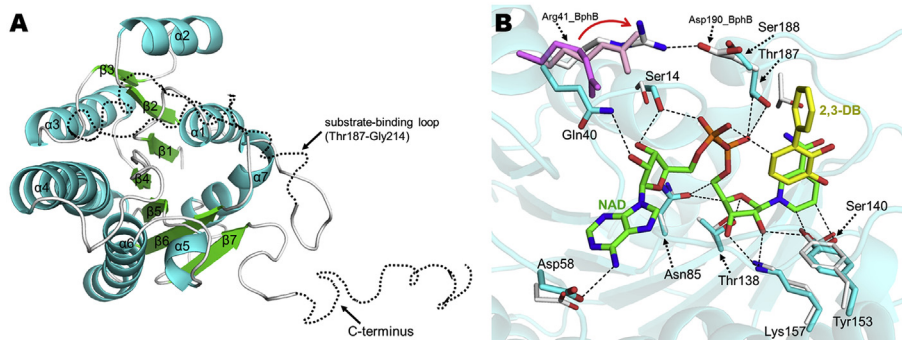


Fig. 2. **A.** Overall structure of NahB. The α helices and β strands are colored as cyan and green, respectively. The flexible substrate-binding loop and the external C-terminus, which is only present in the BphB structure, are presented as black-dotted lines. **B.** Close-up view of the cofactor-binding site of NahB. The residues participating in NAD^+ binding are presented as stick model. The bound NAD^+ and 2,3-DB are also presented as a stick model and colored as green and yellow, respectively. Arg41 in the apo, binary, and ternary structure of BphB are shown as stick models and colored as violet, light pink, and white, respectively. Asp190 in the ternary structure of BphB is shown as stick and colored as white. (For interpretation of the references to colour in this figure legend, the reader is referred to the web version of this article.)

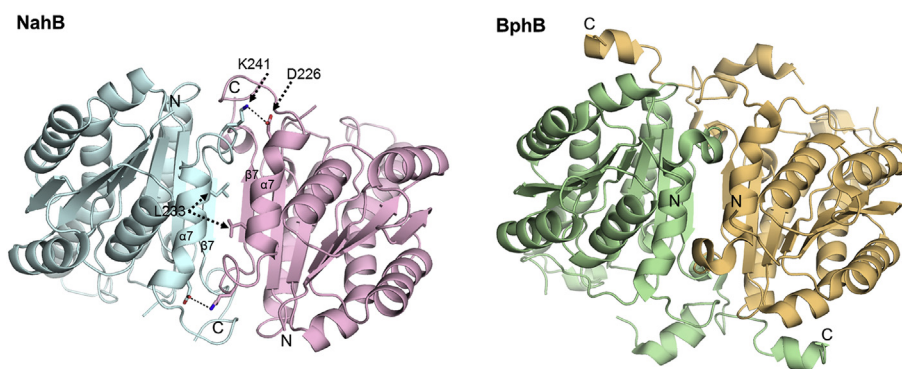


Fig. 3. **Dimer structure of NahB and BphB.** The interface of the two monomers comprising helix $\alpha 7$ and $\beta 7$ is indicated. The residues participating in the dimer interface are shown as stick models.

the two monomers are related to each other by a non-crystallographic two-fold axis (Fig. 3) [20]. The two monomers interact through their respective $\alpha 7$ helix and $\beta 7$ sheet. In NahB, contacts between the helices occur mainly through the hydrophobic interactions, including Leu233. In addition, there exists one salt bridge between Asp226 of $\alpha 7$ and Lys241 of $\alpha 7$ - $\beta 7$. The extended C-terminus in BphB contributes to the formation of the dimer.

3.3. Cofactor- and substrate-binding site

As mentioned above, the enzyme NahB binds to various substrates [16,17]. Therefore, we tried to co-crystallize NahB with 1,2-DN or 2,3-DB as the ligand, which are the final products of NahB-catalyzed reactions. Analysis of the NahB complex structure revealed a clear electron density map for bound NAD^+ . On the other hand, a partial occupancy of 2,3-DB was recognized near the cofactor NAD^+ . The electron density is enough to interpret the structure model of bound 2,3-DB molecule. Superposition of the cofactor-binding site of NahB and BphB revealed that NAD^+ interacts with NahB and BphB in a similar manner (Fig. 2B) [20,32], wherein the nicotinamide ring of NAD^+ interacts with Ser140 and Tyr153. Asn85, Thr138, and Lys157 form hydrogen bonding with the ribose moiety of NAD^+ . The adenosine 5'-diphosphate (ADP) moiety interacts with Ser14, Gln40, Asp58, Thr187, and Ser188. Most of these residues are well conserved in NahB homologs (Fig. S1). However, we observed an additional hydrogen bonding between O2B of NAD^+ and NE2 of Gln40 (Fig. 2B) in NahB as

compared with BphB. Gln40 is a conserved residue in NahB homologs but not BphBs. It is interesting that Arg41 of BphB, which corresponds to Gln40 of NahB, is regarded as an important residue to bind to the substrate-binding loop of BphB [20]. Arg41 of BphB underwent a conformational change upon binding of the substrate, thereby allowing interaction with Asp190 located on the substrate-binding loop (Fig. 2B). Therefore, the newly formed hydrogen bonding makes the substrate-binding loop of BphB ordered. Furthermore, an additional residue Tyr92 imparts rigidity to the substrate-binding loop in the complex structure of BphB [20], which underwent conformational change upon substrate binding. As shown in Fig. 4A, Leu199 of the substrate-binding loop comes in proximity to Tyr92 upon substrate binding. Thus, Tyr92 underwent conformational change to avoid steric hindrance and subsequently formed hydrogen bond with the main chain carboxyl group of Glu202. Glu202 of BphB is located on the substrate-binding loop; therefore, the hydrogen bonding between Tyr92 and Glu202 is one of two important interactions that holds the substrate-binding loop. Comparison between these two residues and the corresponding residues of NahB in the complex structure revealed that Gln40, which interacts with NAD^+ , has no role in holding the substrate-binding loop. On the other hand, Tyr91 of NahB corresponds to Tyr92 of BphB; these two residues adopt similar position upon ligand binding (Fig. 4A). Therefore, we hypothesized that Tyr91 of NahB may undergo a conformational change upon ligand binding. However, the superposition of the apo and complex structure of NahB indicated no significant conformational change of Tyr91. Therefore, it can be postulated that different enzyme-ligand

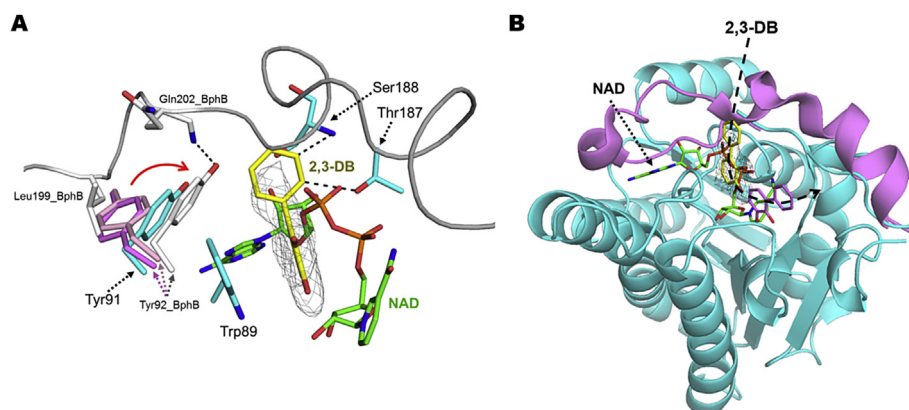


Fig. 4. **A.** The substrate-binding site of NahB. The bound NAD⁺ and 2,3-DB are shown as a stick model and colored as green and yellow, respectively. The substrate-binding loop in the ternary structure of BphB is shown as a ribbon model and colored as gray. Tyr92 in the apo, binary, and ternary structure of BphB are shown as sticks and colored as pink, light pink, and white, respectively. Leu199 and Gln202 in the ternary structure of BphB are shown as sticks and colored as white. The residues that are located around the substrate-binding pocket of NahB are shown as a stick model. The electron density map of 2,3-DB is presented. The map was calculated with $(2|F_o| - |F_c|)$ and contoured at 1.5σ . **B** Structural superposition of NahB (cyan) and BphB (pink). For clarity, only the substrate-binding loop and bound 2,3-DB of BphB are shown. The bound NAD⁺ and 2,3-DB of NahB are presented as stick model and colored as green and yellow, respectively. The predicted binding pathway of the substrate is presented as black-dotted line. (For interpretation of the references to colour in this figure legend, the reader is referred to the web version of this article.)

interactions may be involved in the ordering of substrate-binding loop in NahB as compared with that in BphB.

3.4. Proposed substrate-binding pathway of NahB

In contrast to the rigid substrate-binding loop in the complex structure of BphB, the substrate-binding loop of NahB remains disordered even in the presence of the substrate. Furthermore, the superposition of the complex structure of NahB and BphB revealed that 2,3-DB occupies different positions in NahB and BphB (Fig. 4B). The close-up view of the substrate-binding site of NahB revealed that both residues Thr187 and Ser188 located at the distal end of the loop form hydrogen bond with 2,3-DB. A benzene ring of the bound 2,3-DB is sandwiched between Trp89 and nicotinamide ring of NAD⁺ (Fig. 4A). As shown in Fig. 4B, 2,3-DB binds adjacent to the substrate-binding loop of NahB and is distant to the active site, while it binds at the active site in the cavity of BphB, which is covered by the substrate-binding loop. Therefore, NahB structure presents the crystallographic snapshot for the entry or release of the product in the enzyme-ligand binding process. The substrate-binding process in BphB is as follows: NAD⁺ binds to the cofactor-binding site without inducing closure of the cavity. This is followed by the entry of the substrate that induces conformational change in the substrate-binding loop, resulting in the closure of the active site [20,33]. The flexibility of the substrate-binding loop presumably plays an important role in accommodating diverse substrates. Taken together, we suggest that the substrate may bind to the first-binding site near the distal part of the substrate-binding loop at the early stage, as shown in the complex structure of NahB. There may exist a process of dynamic recognition between the substrate-binding loop and the substrate. The substrate may subsequently move to the active site for catalysis. During the enzyme reaction, the substrate-binding loop covers the active site to prevent the release of the substrate and may become flexible again to release the product.

Funding

This work was supported by a 'Polar Genomics 101 Project' grant (PE17080) funded by the Korea Polar Research Institute (KOPRI).

Acknowledgements

We would like to thank the staff at the BL-5C of the Pohang Accelerator Laboratory (Pohang, Korea) for their help with data collection.

Transparency document

Transparency document related to this article can be found online at <http://dx.doi.org/10.1016/j.bbrc.2017.07.089>

Appendix A. Supplementary data

Supplementary data related to this article can be found at <http://dx.doi.org/10.1016/j.bbrc.2017.07.089>

References

- [1] Y. Kasai, K. Shindo, S. Harayama, N. Misawa, Molecular characterization and substrate preference of a polycyclic aromatic hydrocarbon dioxygenase from *Cycloclasticus* sp strain A5, *Appl. Environ. Microbiol.* 69 (2003) 6688–6697.
- [2] F. Volkering, A.M. Breure, A. Sterkenburg, J.G. Vanandel, Microbial-degradation of polycyclic aromatic-hydrocarbons - effect of substrate availability on bacterial-growth kinetics, *Appl. Microbiol. Biotechnol.* 36 (1992) 548–552.
- [3] W.M. Baird, L.A. Hooven, B. Mahadevan, Carcinogenic polycyclic aromatic hydrocarbon-DNA adducts and mechanism of action, *Environ. Mol. Mutagen.* 45 (2005) 106–114.
- [4] H. Habe, T. Omori, Genetics of polycyclic aromatic hydrocarbon metabolism in diverse aerobic bacteria, *Biosci. Biotechnol. Biochem.* 67 (2003) 225–243.
- [5] J.G. Mueller, P.J. Chapman, P.H. Pritchard, Action of a fluoranthene-utilizing bacterial community on polycyclic aromatic hydrocarbon components of creosote, *Appl. Environ. Microbiol.* 55 (1989) 3085–3090.
- [6] R. Preuss, J. Angerer, H. Drexler, Naphthalene - an environmental and occupational toxicant, *Int. Archives Occup. Environ. Health* 76 (2003) 556–576.
- [7] D. Brusick, Critical assessment of the genetic toxicity of naphthalene, *Regul. Toxicol. Pharmacol.* 51 (2008) S37–S42.
- [8] K.M. Yen, C.M. Serdar, Genetics of naphthalene catabolism in *Pseudomonas*, *Crc Crit. Rev. Microbiol.* 15 (1988) 247–268.
- [9] S.L. Fuenmayor, M. Wild, A.L. Boyes, P.A. Williams, A gene cluster encoding steps in conversion of naphthalene to gentisate in *Pseudomonas* sp. strain U2, *J. Bacteriol.* 180 (1998) 2522–2530.
- [10] M.A. Schell, P.H. Brown, S. Raju, Use of saturation mutagenesis to localize probable functional domains in the *nahr* protein, a *lysR*-type transcription activator, *J. Biol. Chem.* 265 (1990) 3844–3850.
- [11] E. Ahn, K.Y. Choi, B.S. Kang, G.J. Zylstra, D. Kim, E. Kim, Salicylate degradation by a cold-adapted *Pseudomonas* sp, *Ann. Microbiol.* 67 (2017) 417–424.
- [12] L. Tomas-Gallardo, H. Gomez-Alvarez, E. Santero, B. Floriano, Combination of degradation pathways for naphthalene utilization in *Rhodococcus* sp strain

- TFB, *Microb. Biotechnol.* 7 (2014) 100–113.
- [13] N.Y. Zhou, S.L. Fuenmayor, P.A. Williams, Nag genes of *Ralstonia* (formerly *Pseudomonas*) sp strain U2 encoding enzymes for gentisate catabolism, *J. Bacteriol.* 183 (2001) 700–708.
- [14] R.M. Jones, B. Britt-Compton, P.A. Williams, The naphthalene catabolic (nag) genes of *Ralstonia* sp strain U2 are an operon that is regulated by NagR, a LysR-type transcriptional regulator, *J. Bacteriol.* 185 (2003) 5847–5853.
- [15] B.D. Ensley, D.T. Gibson, A.L. Laborde, Oxidation of naphthalene by a multi-component enzyme system from *Pseudomonas* sp. strain NCIB 9816, *J. Bacteriol.* 149 (1982) 948–954.
- [16] T.R. Patel, D.T. Gibson, Purification and properties of (plus)-cis-naphthalene dihydrodiol dehydrogenase of *Pseudomonas putida*, *J. Bacteriol.* 119 (1974) 879–888.
- [17] D. Barriault, M. Vedadi, J. Powlowski, M. Sylvestre, Cis-2,3-dihydro-2,3-dihydroxybiphenyl dehydrogenase and cis-1,2-dihydro-1,2-dihydroxynaphthalene dehydrogenase catalyze dehydrogenation of the same range of substrates, *Biochem. Biophysical Res. Commun.* 260 (1999) 181–187.
- [18] H. Raschke, T. Fleischmann, J.R. Van Der Meer, H.P. Kohler, Cis-chlorobenzene dihydrodiol dehydrogenase (TcbB) from *Pseudomonas* sp. strain P51, expressed in *Escherichia coli* DH5alpha(pTCB149), catalyzes enantioselective dehydrogenase reactions, *Appl. Environ. Microbiol.* 65 (1999) 5242–5246.
- [19] Y. Jouanneau, C. Meyer, Purification and characterization of an arene cis-dihydrodiol dehydrogenase endowed with broad substrate specificity toward polycyclic aromatic hydrocarbon dihydrodiols, *Appl. Environ. Microbiol.* 72 (2006) 4726–4734.
- [20] S. Dhindwal, D.N. Patil, M. Mohammadi, M. Sylvestre, S. Tomar, P. Kumar, Biochemical studies and ligand-bound structures of biphenyl dehydrogenase from *Pandoraea pnomenusa* strain B-356 reveal a basis for broad specificity of the enzyme, *J. Biol. Chem.* 286 (2011) 37011–37022.
- [21] C.L. Lin, F.T. Shen, C.C. Tan, C.C. Huang, B.Y. Chen, A.B. Arun, C.C. Young, Characterization of *Gordonia* sp strain CC-NAPH129-6 capable of naphthalene degradation, *Microbiol. Res.* 167 (2012) 395–404.
- [22] Z. Otwinowski, W. Minor, Processing of X-ray diffraction data collected in oscillation mode, *Macromolecular Crystallography, Pt A* 276 (1997) 307–326.
- [23] A. Vagin, A. Teplyakov, Molecular replacement with MOLREP, *Acta Crystallogr. Sect. D-Biological Crystallogr.* 66 (2010) 22–25.
- [24] G.N. Murshudov, P. Skubak, A.A. Lebedev, N.S. Pannu, R.A. Steiner, R.A. Nicholls, M.D. Winn, F. Long, A.A. Vagin, REFMAC5 for the refinement of macromolecular crystal structures, *Acta Crystallogr. Sect. D-Biological Crystallogr.* 67 (2011) 355–367.
- [25] P. Emsley, B. Lohkamp, W.G. Scott, K. Cowtan, Features and development of coot, *Acta Crystallogr. Sect. D-Biological Crystallogr.* 66 (2010) 486–501.
- [26] V.B. Chen, W.B. Arendall, J.J. Headd, D.A. Keedy, R.M. Immormino, G.J. Kapral, L.W. Murray, J.S. Richardson, D.C. Richardson, MolProbity: all-atom structure validation for macromolecular crystallography, *Acta Crystallogr. Sect. D-Biological Crystallogr.* 66 (2010) 12–21.
- [27] The PyMOL Molecular Graphics System, Version 1.2r3pre, Schrödinger, LLC.
- [28] H. Raschke, T. Fleischmann, J.R. Van der Meer, H.P.E. Kohler, Cis-Chlorobenzene dihydrodiol dehydrogenase (TcbB) from *Pseudomonas* sp strain P51, expressed in *Escherichia coli* DH5 alpha(pTCB149), catalyzes enantioselective dehydrogenase reactions, *Appl. Environ. Microbiol.* 65 (1999) 5242–5246.
- [29] H.D. Simpson, J. Green, H. Dalton, Purification and some properties of a novel heat-stable cis-toluene dihydrodiol dehydrogenase, *Biochem. J.* 244 (1987) 585–590.
- [30] M. Sylvestre, Y. Hurtubise, D. Barriault, J. Bergeron, D. Ahmad, Characterization of active recombinant 2,3-dihydro-2,3-dihydroxybiphenyl dehydrogenase from *Comamonas testosteroni* B-356 and sequence of the encoding gene (bphB), *Appl. Environ. Microbiol.* 62 (1996) 2710–2715.
- [31] L. Holm, P. Rosenstrom, Dali server: conservation mapping in 3D, *Nucleic Acids Res.* 38 (2010) W545–W549.
- [32] M. Hulsmeyer, H.J. Hecht, K. Niefind, B. Hofer, L.D. Eltis, K.N. Timmis, D. Schomburg, Crystal structure of cis-biphenyl-2,3-dihydrodiol-2,3-dehydrogenase from a PCB degrader at 2.0 angstrom resolution, *Protein Sci.* 7 (1998) 1286–1293.
- [33] A. Andersson, D. Jordan, G. Schneider, Y. Lindqvist, A flexible lid controls access to the active site in 1,3,8-trihydroxynaphthalene reductase, *FEBS Lett.* 400 (1997) 173–176.